

# Prediction of Catalytic Converter Efficiency in Natural Gas Engine for Nitrogen Monoxide and Carbon Monoxide Emission Control

<sup>1</sup>Cheong YK, <sup>2</sup>Chuah L, <sup>1</sup>NM Adam, <sup>3\*</sup>Basharia A. A. Yousef

<sup>1</sup>Alternative and Renewable Energy Laboratory, Institute of Advanced Technology, Universiti Putra Malaysia, 43400 UPM Serdang, Malaysia

<sup>2</sup>Department of Chemical and Environmental Engineering, Faculty of Engineering, Universiti Putra Malaysia, 43400 UPM Serdang, Malaysia.

<sup>3\*</sup>Department of Mechanical Engineering, College of Engineering and Architecture, University of Bahri, Khartoum North, Sudan, P.O. Box 13104, Khartoum, Sudan

<sup>3\*</sup>E-mail: [bashria@yahoo.com](mailto:bashria@yahoo.com), Tel.: 00249-918641746

**Abstract-** The objective of this study is to carry out simulation on catalytic converter design and efficiency in a cold start natural gas engine for nitrogen monoxide and carbon monoxide emission control. CFD code FLUENT 6.0 was used for prediction of catalytic converter light-off temperature and efficiency. Cold start and light-off temperatures is the acceptable worst scenario for compressed natural gas (CNG) engine pollutants abatement in order to achieve low emission vehicle. The simulation result was then verified via experimental data published in literature. The simulation of catalytic converter light-off temperature for NO and CO were proved to be satisfactory when compared to presented experimental result. The light off temperature for NO conversion at 583 K and CO conversion at 523 K and all within measured values from literature. This work possible to simulate combustion using CFD software.

**Keywords-** Catalytic converter; Natural gas vehicle; Nitrogen monoxide; Carbon monoxide.

## 1. Introduction

Catalyst is a substance which helps to affect the rate of chemical reaction by lowering activation energy of the chemical reaction while itself not undergoing any change. Catalytic converter of automobiles contains catalysts such as platinum (Pt), rhodium (Rd) and palladium (Pd) to treat exhaust air. Vehicle catalytic converters used in the 1970s and 1980s, oxidized unburned harmful hydrocarbons (uHC) and carbon monoxide (CO) into water (H<sub>2</sub>O) and carbon dioxide (CO<sub>2</sub>). They are called two-way catalytic converter. A three-way catalytic converter (TWCC) is a triple purpose converter. It reduces nitrous oxides (NO<sub>x</sub>) into nitrogen (N<sub>2</sub>) and oxygen (O<sub>2</sub>). And, like the two-way converter, it oxidizes unburned harmful hydrocarbons and carbon monoxide into water and carbon dioxide. Modelling and simulation works of catalytic converters has been done since 1970s. Early simulation works by Kuo et al. (1971), Heck et al. (1976), Young and Finlayson (1976), and Oh and Cavendish (1982) were in one-dimensional models. With computer development in the 1980s, Chen et al. (1988), Zygourakis (1989), Hayes et al. (1992) were among the pioneers to model catalytic converters in two-dimensional

models. Empirical models done on catalytic converters simulation were in steady state models, transient models and light-off criteria on cold start engine. Detailed chemical reactions in catalytic converters are too complex to be modelled. Chemical reactions involving CO, NO, ethylene, methane, propene and acetylene were normally selected for modelling purposes.

Now days the solution of Navier-Stokes equations by numerical techniques has been made possible by the advent of powerful software compiler, opening avenues towards the calculation of complicated flow fields in cyclone with relative ease via computational fluid dynamics software such as FLOVENT, PHOENICS. More research on cold start is done compared to steady state condition. Seimund et al. (1996), Taylor (1999), Koltsakis & Stamatelos (1999), Jirat et al. (2001), Koci et al. (2003) and Tsinoglou et al. (2003) are among those who conducted simulation of catalytic converter in steady state condition. Taylor, (1999) and Jirat et al. (2001) used simulated effect of high temperatures on catalytic converter behavior. Koci et al. (2003) and Koltsakis and Stamatelos (1999) simulated the characteristic and effects of NO<sub>x</sub> and O<sub>2</sub> storage respectively under periodic temperature and lean/rich operations.

Hoebink et al. (1999) simulated and confirmed the light-off is in the sequence of H<sub>2</sub>, CO and propene. Harmsen et al. (1999), Jirat et al. (2001) and Harmsen et al. (2001) simulated the kinetics and effects of various uHC such as ethylene and acetylene on the reactions inside catalytic converter under cold start condition. Jeong and Kim (2002), Chakravarty et al. (2003), Tsinoglou et al. (2003) and Shuai & Wang (2004) studied and simulated effects of physical flow distribution into the monolith on the catalytic performance during cold start. Shuai and Wang (2004) found that positioning an inlet cone with certain angle can improve the light-off characteristics due to a more evenly distributed velocity and temperature over the monolith inlet surface. Ramanathan et al. (2004) simulated the effect of catalyst loading and catalyst distribution along the channel length at cold start. He found that a two zone catalyst distribution with more catalyst near the inlet reduces the cumulative emissions compared to the case of uniform catalyst loading.

All catalytic converter simulation and modeling works for steady state and cold start mentioned above were done for petrol engines emission abatement. There is no simulation work done for compressed natural gas vehicle emission abatement, neither in steady state nor cold start condition. Also, there is no modeling work on surface reaction for catalytic converter using CFD FLUENT 6.0. This work was done to fill the gap in knowledge in simulation and modeling of compressed natural gas vehicle emission abatement.

## 2. Theoretical Analysis

For all flows in chemical reaction modeling, FLUENT solves conservation equations for chemical species. FLUENT predicts the local mass fraction of each species, Y<sub>i</sub>, through the solution of convection-diffusion equation for the i<sup>th</sup> species. The conservation equation takes the following general form

$$\frac{\partial(\rho Y_i)}{\partial t} + \nabla \cdot (\rho \bar{v} Y_i) = -\nabla \cdot \bar{J}_i + R_i + S_i \quad (1)$$

Where

- Y<sub>i</sub> Local mass fraction of each species
- R<sub>i</sub> The net rate of production by chemical reaction
- S<sub>i</sub> The rate of creation by addition from the dispersed phase
- J<sub>i</sub> Diffusion flux of species i
- ρ Gas density, g/cm<sup>3</sup>
- $\bar{v}$  Velocity, cm/s

Since the mass fraction of the species must sum to unity, the N<sup>th</sup> mass fraction is determined as one minus the sum of the N-1 solved mass fractions.

In Equation (1), J<sub>i</sub> is the diffusion flux of species i, which arises due to concentration gradients. By default, FLUENT uses the dilute approximation, under which the diffusion flux can be written as

$$\bar{J}_i = -\rho D_{i,m} \nabla Y_i \quad (2)$$

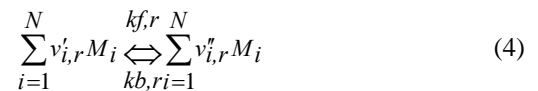
Here D<sub>i,m</sub> is the diffusion coefficient for species i in the mixture.

The laminar finite-rate model computes the chemical source terms using Arrhenius expressions, and ignores the effects of turbulent fluctuations. The net source of chemical species i due to reaction R<sub>i</sub> is computed as the sum of the Arrhenius reaction sources over the N<sub>R</sub> reactions that the species participate in:

$$R_i = M_i \sum_{r=1}^{N_R} \hat{R}_{i,r} \quad (3)$$

Reaction may occur in the continuous phase between continuous-phase species only, or at wall surfaces resulting in the surface deposition or evolution of a continuous-phase species.

Consider the r<sup>th</sup> reaction written in general form as follows:



Where N is number of chemical species in the system, v'<sub>i,r</sub> is stoichiometric coefficient for reactant i in reaction r, v''<sub>i,r</sub> is stoichiometric coefficient for product i in reaction r, M<sub>i</sub> denotes symbol denoting species I, k<sub>f,r</sub> is forward rate constant for reaction r and k<sub>b,r</sub> is backward rate constant for reaction r.

Equation (4) is valid for both reversible and non-reversible reactions. Reactions in FLUENT are non-reversible by default. For non-reversible reactions, the backward rate constant, k<sub>b,r</sub>, is omitted. The summations in Equation (4) are for all chemical species in the system, but only species that appear as reactants or products will have non-zero stoichiometric coefficients. Hence, species that are not involved will not appear in the equation.

The molar rate of creation/destruction of species i in reaction r (  $\hat{R}_{i,r}$  in Equation (3)) is given by

$$\hat{R}_{i,r} = \Gamma(v''_{i,r} - v'_{i,r}) \left( k_{f,r} \prod_{j=1}^{N_r} [C_{j,r}]^{n'_{j,r}} - k_{b,r} \prod_{j=1}^{N_r} [C_{j,r}]^{n''_{j,r}} \right) \quad (5)$$

Where N<sub>r</sub> is number of chemical species in reaction r, C<sub>j,r</sub> is molar concentration of each reactant and product species j in reaction r (kgmol/cm<sup>3</sup>), n'<sub>j,r</sub> is forward rate exponent for each reactant and product species j in reaction r and n''<sub>j,r</sub> is backward rate exponent for each reactant and product species j in reaction r.

$\Gamma$  represents the net effect of third bodies on the reaction rate. This term is given by

$$\Gamma = \sum_j^{Nr} \gamma_{j,r} C_j \quad (6)$$

where  $\gamma_{j,r}$  is the third-body efficiency of the  $j$ th species in the  $r$ th reaction. The third-body effect in the reaction rate calculation has been omitted.

The forward rate constant for reaction  $r$ ,  $k_{f,r}$ , is computed using the Arrhenius expression

$$k_{f,r} = A_r T^{\beta_r} e^{-E_r / RT} \quad (7)$$

Where  $A_r$  is pre-exponential factor (consistent units),  $\beta_r$  is temperature exponent (dimensionless),  $E_r$  is activation energy for the reaction (J/kgmol) and  $R$  is universal gas constant (J/kgmol-K). Values for  $v'_{i,r}$ ,  $v''_{i,r}$ ,  $n'_{j,r}$ ,  $n''_{j,r}$ ,  $A_r$ ,  $E_r$ , and  $\gamma_{j,r}$ , optionally, is to be input during the problem definition in FLUENT.

For reversible reaction, the backward rate constant for reaction  $r$ ,  $k_{b,r}$ , is computed from the forward rate constant using the following relation:

$$k_{b,r} = \frac{k_{f,r}}{K_r} \quad (8)$$

where  $K_r$  is the equilibrium constant for the  $r$ th reaction, computed from

$$K_r = e^{\left( \frac{\Delta S_r^0}{R} - \frac{\Delta H_r^0}{RT} \right) \left( \frac{p_{atm}}{RT} \right)^{\sum_{i=1}^{Nr} (v''_{i,r} - v'_{i,r})}} \quad (9)$$

where  $p_{atm}$  denotes atmospheric pressure (101325 Pa). The term within the exponential function represents the change in Gibbs free energy, and its components are computed as follows:

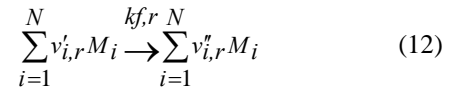
$$\frac{\Delta S_r^0}{R} = \sum_{i=1}^N (v''_{i,r} - v'_{i,r}) \frac{S_i^0}{R} \quad (10)$$

$$\frac{\Delta H_r^0}{RT} = \sum_{i=1}^N (v''_{i,r} - v'_{i,r}) \frac{h_i^0}{RT} \quad (11)$$

where  $S_i^0$  and  $h_i^0$  are the standard-state entropy and standard-state enthalpy (heat of formation). These values are specified in FLUENT as properties of the mixture material.

For gas-phase reactions, the reaction rate is defined on a volumetric basis and the rate of creation and destruction of chemical species becomes a source term in the species conservation equations. The rate of deposition is governed by both chemical kinetics and the diffusion rate from the fluid to the surface. Wall surface reactions thus create sources (and sinks) of chemical species in the bulk phase and determine the rate of deposition of surface

species. For the  $r$ th wall surface reaction written in general form as follows:



where  $N$  is number of chemical species in the system,  $v'_{i,r}$  is stoichiometric coefficient for reactant  $i$  in reaction  $r$ ,  $v''_{i,r}$  is stoichiometric coefficient for product  $i$  in reaction  $r$ ,  $M_i$  denotes symbol denoting species  $i$ ,  $k_{f,r}$  is forward rate constant for reaction  $r$  and  $k_{b,r}$  is backward rate constant for reaction  $r$ .

The summations in Equation (12) are for all chemical species in the system, but only species involved as reactants or products will have non-zero stoichiometric coefficients. Hence, species that are not involved will not appear in the equation.

The molar rate of creation/destruction of species  $i$  in reaction  $r$  ( $\hat{R}_{i,r}$  in Equation (5)) is given by

$$\hat{R}_{i,r} = (v''_{i,r} - v'_{i,r}) \left( k_{f,r} \prod_{j=1}^{Nr} [C_{j,r}]^{n'_{j,r}} \right) \quad (13)$$

where  $N_r$  is number of chemical species in reaction  $r$ ,  $C_{j,r}$  is molar concentration of each reactant and product species  $j$  in reaction  $r$  (kgmol/cm<sup>3</sup>),  $n'_{j,r}$  is forward rate exponent for each reactant and product species  $j$  in reaction  $r$ .

The forward rate constant for reaction  $r$ ,  $k_{f,r}$ , is computed using the Arrhenius expression

$$k_{f,r} = A_r T^{\beta_r} e^{-E_r / RT} \quad (14)$$

Where  $A_r$  is pre-exponential factor (consistent units),  $\beta_r$  is temperature exponent (dimensionless),  $E_r$  is activation energy for the reaction (J/kgmol) and  $R$  is universal gas constant (J/kgmol-K). User will provide values for  $v'_{i,r}$ ,  $v''_{i,r}$ ,  $n'_{j,r}$ ,  $A_r$ , and  $E_r$ .

### 3. Methodology

The study involved the modelling and simulation of catalytic converter using two dimensional CFD. The CFD modelling and simulation are carried out via a commercial CFD code name FLUENT 6.0. FLUENT CFD package includes the following products:

- FLUENT, the solver.
- prePDF, the preprocessor for modeling non-premixed combustion in FLUENT.
- GAMBIT, the preprocessor for geometry modeling and mesh generation.

- TGrid, an additional preprocessor that can generate volume meshes from existing boundary meshes.
- filters (translators) for import of surface and volume meshes from CAD/CAE packages such as ANSYS, CGNS, I-DEAS, NASTRAN, PATRAN, and others.

Figure 1 shows the organisational structure of these components.

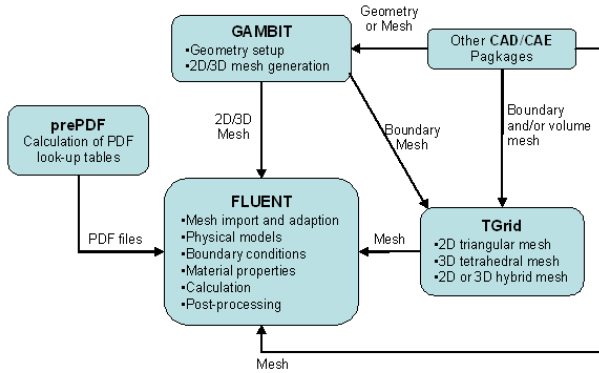


Figure 1. Basic Program Structure

Once a grid has been read into FLUENT, all remaining operations are performed within the solver. These include setting boundary conditions, defining fluid properties, executing the solution, refining the grid, and viewing and post processing the results. Figure 2 shows the overall steps in CFD analysis.

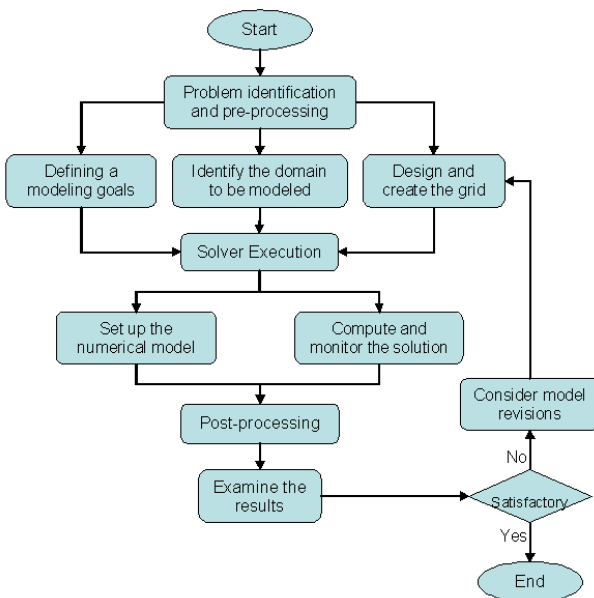


Figure 2. Steps on CFD Analysis

### 3.1 CFD Modelling of Catalytic Converter

#### 3.1.1 Scope, Boundary Conditions and Assumptions

The catalytic converter type chosen for the two dimensional modelling work is the monolithic type with 400 cpsi, which is similar to the catalytic converter used by Chatterjee et al. (2001) in their experiment. According to Heck et al. (2002) and Chatterjee et al. (2001) almost

all automobiles today are equipped more with monolithic catalysts than beaded type catalysts. In the CFD modelling of three way catalytic converter, the first step is a numerical grid creation (Fig. 3). The computational quadrilateral grid was created using Gambit 2.0 with at least 14352 nodes to yield a reasonable prediction. Since the physical catalytic converter is rectangular in shape, simple quadrilateral grid was used. The second step was a solver execution in Fluent 6.0 in which the boundary condition, material properties and calculation took place.

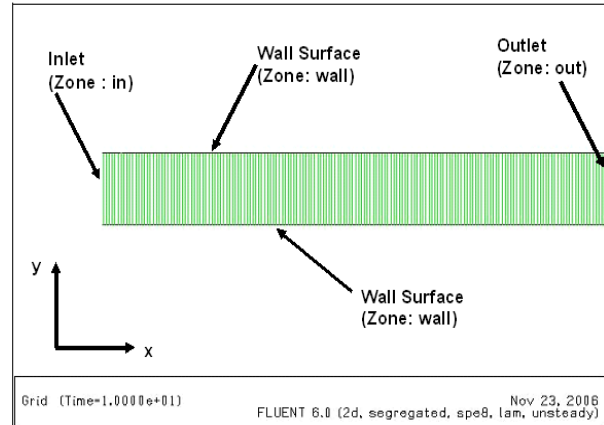


Figure 3. Computational Grid Creation

The catalysts modelled are Platinum (Pt) and Rhodium (Rd). The exhaust gas produced by gas engine under stoichiometric condition at cold start and assumed at constant 750K at inlet of the catalytic converter, similar temperature in experiment conducted done by Chan and Hoang (1990). The gas density is assumed to be incompressible ideal gas condition with gas heat capacity abiding gas mixing law. Absolute pressure is at 1 atmosphere. The boundary conditions for this simulation module are summarised as in Table 1.

Table 1. Boundary Conditions of the Catalytic Converter Model

No	Zone	Type	Parameter
1	exhaust	Fluid	NGV exhaust
2	in	velocity-inlet	Velocity Magnitude : 0.5m/s Temperature : 750K
3	wall	Wall	Temperature : 300K Free stream Temperature : 300K External Radiation Temperature : 300K
4	out	Outflow	Flow rate weighting : 1

#### 3.1.2 Chemical Reactions

Chemical reactions in the monolith catalytic converter are very complicated. There are hundreds of reactions that occur inside a catalytic converter (Chan and Hoang, 1999). In this work, only reactions involving NO and CO are considered in the simulation. Even the NO and CO reactions take place in many complicated steps. The overall chemical reactions, rate of expression and constant as mentioned in equation 7 and 14 which based on the works of Koltsakis (2003) in Table 2 are keyed into the

Fluent 6.0. The reactions in Table 2 are basic and global reactions in a catalytic converter according to Heck et al. (2002) and Chatterjee et al. (2001). The gas compositions of the compressed NGV exhaust gas from Ristovski et al. (2000) as shown in Table 3 were used as inlet of reactants for the catalytic converter in this work. N<sub>2</sub> quantity is the balance of the total quantity in default.

**Table 2. Chemical Reaction, Rate of Expression and Constant Input into Fluent**

No	Reaction	Forward Expression	Rate	A <sub>r</sub>	β <sub>r</sub>	E <sub>r</sub> (J/kgmol)	x
1	2CO + 2NO → 2CO <sub>2</sub> + N <sub>2</sub>	$k_{f,r} = A_r T^r \exp^{-E_r/RT}$	$\exp^{-L}$	$1.0 \times 10^{14}$	-1.83	$8.0 \times 10^7$	x
2	CO + NO → CO <sub>2</sub> + N <sub>2</sub> O	$k_{f,r} = A_r T^r \exp^{-L}$	$\exp^{-L}$	$2.0 \times 10^{14}$	-1.83	$8.0 \times 10^7$	x
3	CO + N <sub>2</sub> O → CO <sub>2</sub> + N <sub>2</sub>	$k_{f,r} = A_r T^r \exp^{-L}$	$\exp^{-L}$	$7.0 \times 10^{13}$	0.00	$1.2 \times 10^8$	x
4	2H <sub>2</sub> + 2NO → 2H <sub>2</sub> O + N <sub>2</sub>	$k_{f,r} = A_r T^r \exp^{-L}$	$\exp^{-L}$	$1.0 \times 10^{16}$	-1.00	$8.5 \times 10^7$	x
5	CO + H <sub>2</sub> O → CO <sub>2</sub> + H <sub>2</sub>	$k_{f,r} = A_r T^r \exp^{-L}$	$\exp^{-L}$	$5.0 \times 10^9$	-1.00	$5.0 \times 10^7$	x

**Table 3. Composition of the compressed NGV Exhaust Gas (Ristovski et al., 2000)**

No	Gas	Composition
1	CO <sub>2</sub>	7.26 %
2	O <sub>2</sub>	3 %
3	CO	428 ppm
4	H <sub>2</sub> O	15 %
5	NO	195 ppm
6	NO <sub>2</sub>	5 ppm
7	N <sub>2</sub>	74.72%

**3.1.3 Solver**

The simulation is then solved with a 2-D, segregated, laminar flow, unsteady state solver and first order implicit in FLUENT to reach the convergence. Figure 4 shows a typical iteration residual plot for catalytic converter simulation. The iteration is carried out until the convergence is reached (Figs. 4 and 5). The convergence residual for x-velocity, y-velocity, continuity and all species were monitored to  $1 \times 10^{-3}$  convergence criterion whereas for energy was monitored to  $1 \times 10^{-6}$  convergence criterion.

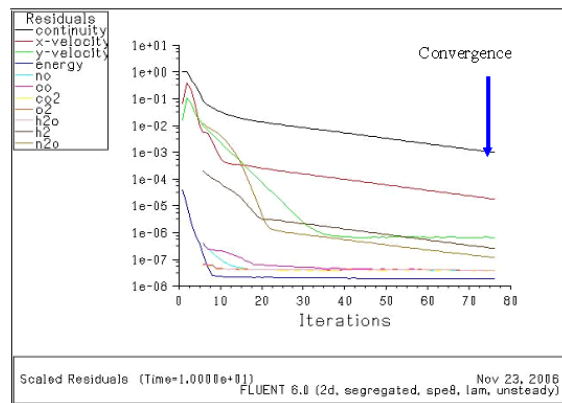


**Figure 4. Iteration (Solver execution)**

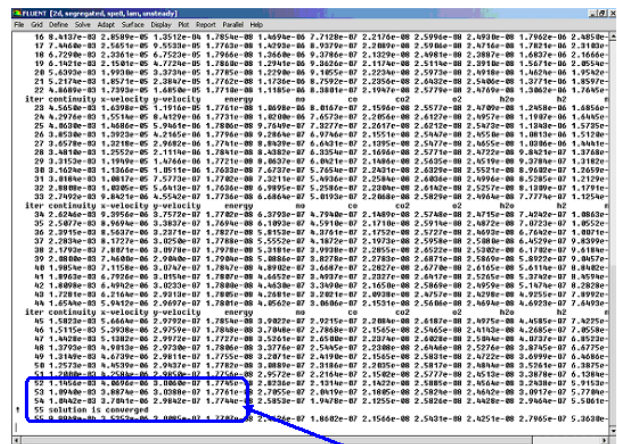


**Figure 5. Convergence**

After the iteration converged, the mass fraction contour of NO, CO, CO<sub>2</sub>, H<sub>2</sub>O, N<sub>2</sub>, N<sub>2</sub>O and H<sub>2</sub> in the catalytic converter can be obtained. The iteration process until convergence took about 16 minutes.

**4. Results and Discussion**

**4.1 Temperature Profile**

The result of CFD Fluent 6.0 simulation on temperature profile of the exhaust gas at front and at rear of the catalytic converter is shown in Figure 6. The simulated calculation result shows similar pattern with the experimental data from Chan and Hoang (1999). Both front and rear temperatures of the catalytic converter eventually meet each other at 750K.

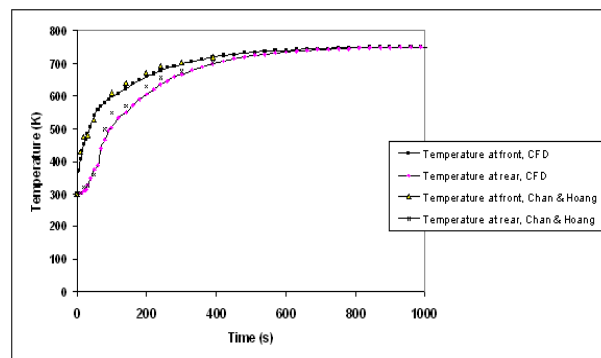


**Figure 6. CFD Simulation of Temperature Profile of Exhaust Gas at Front and at Rear of Catalytic Converter Subject to Cold Start Exhaust Gas at 750 K**

temperature as reported by Chan and Hoang (1999) and Chatterjee et al. (2001).

**4.1.1 Conversion Efficiency Prediction**

As the exhaust gradually warms, it reaches a temperature high enough to initiate the catalytic reactions. This is referred as the light-off temperature (Heck et al., 2002). The light-off temperatures of three way catalytic converters are in the range of 523K (250°C) to 613K (340°C) according to Burch et al. (1995). In this simulation, the light-off temperature is approximately 523K (250°C) for CO and 583K (310°C) for NO (Figures 7 - 10) which is in the range of the experimental data of Chatterjee et al. (2001).

The contours of CO mass fraction and NO mass fraction in the catalytic converter simulation results are shown in Figure 8. The CFD simulation shows that the CO reaction begin first and followed by NO reaction which is agree well with Heck et al. (2002). The mass fraction contours in Figure 8 at t = 50 s shows that CO conversion has started while NO conversion has not begun. This corresponds to cold-starting temperature of 523K. At t = 120 s, NO conversion is taking place, when the corresponding temperature is about 583K.

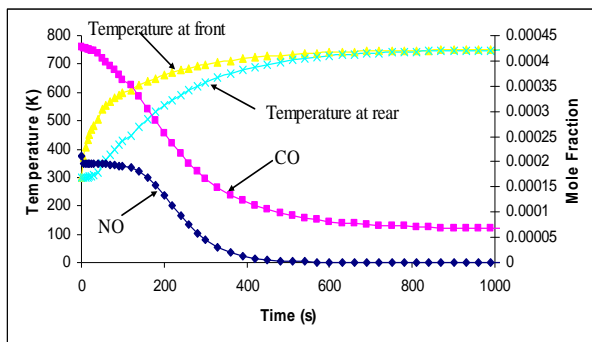


**Figure 7. Profile of Monolith Temperature, CO and NO at Monolith Outlet During Cold Start**

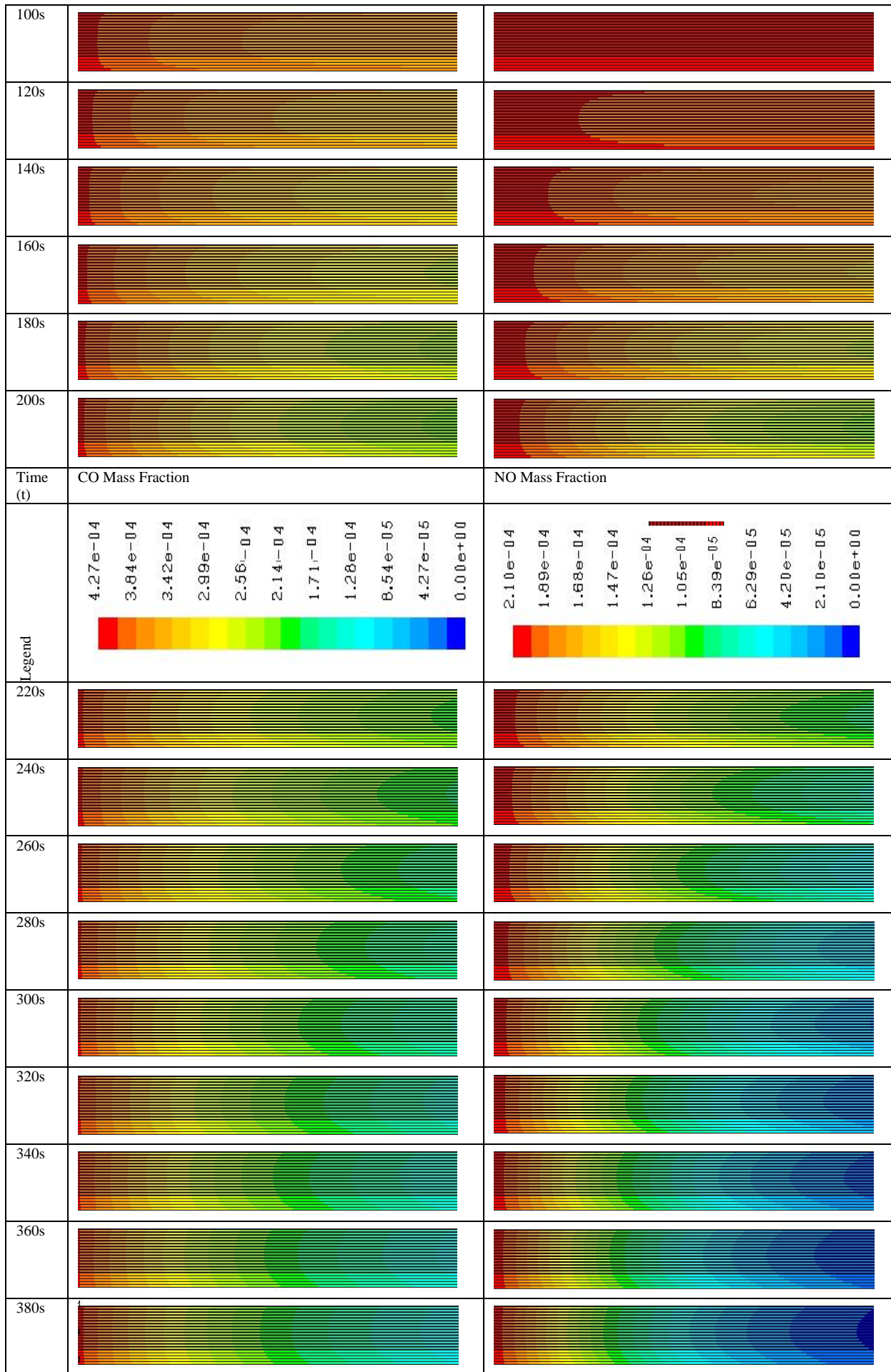
Figures 9 and 10 show the conversion efficiency profile of NO and CO respectively. The conversion of NO begins exponentially from 583K and begins to saturate at 673K to a conversion of 99% as in Figure 9.

Figure 7 shows the reduction profile of CO and NO mole fraction during the cold start. The simulation results show that at the beginning of the cold start, the NO and CO have a high mole fraction in the exhaust gas at the outlet of the catalytic converter. The high quantity of CO and NO emission at this moment is due to low chemical reaction rate because of low temperature of catalytic converter. The CO and NO conversion begin significantly after the catalytic converter reached temperature of approximately 523K and 583K which is the light-off

Simulation results as plotted in Figure 9 showed that the predicted conversion rates of NO in CFD agree well with the experimental data from Chatterjee et al. (2001). The conversion of CO begins exponentially from 523K and begins to saturate at 673K to a conversion of 84% as in Figure 10.

Visual comparison of the simulated results and Chatterjee et al. (2001) data as in Figure 10. It can be concluded that the predicted conversion rates of CO in CFD did not agree completely with the experimental data from Chatterjee et al. (2001). The large deviation of predicted CO conversion profile compared to experimental data might be due to exclusion of hydrocarbon reactions in this simulation. In the absence of omitted hydrocarbon species in the simulation, more free catalysts surface are available for CO conversion, hence the simulated CO conversion rate is higher than experimental data as shown in Figure 10.

Time (t)	CO Mass Fraction	NO Mass Fraction
Legend	4.27e-04 3.84e-04 3.42e-04 2.99e-04 2.56e-04 2.14e-04 1.71e-04 1.28e-04 8.54e-05 4.27e-05 0.00e+00	2.10e-04 1.89e-04 1.68e-04 1.47e-04 1.26e-04 1.05e-04 8.39e-05 6.29e-05 4.20e-05 2.10e-05 0.00e+00
20s		
50s		
80s		



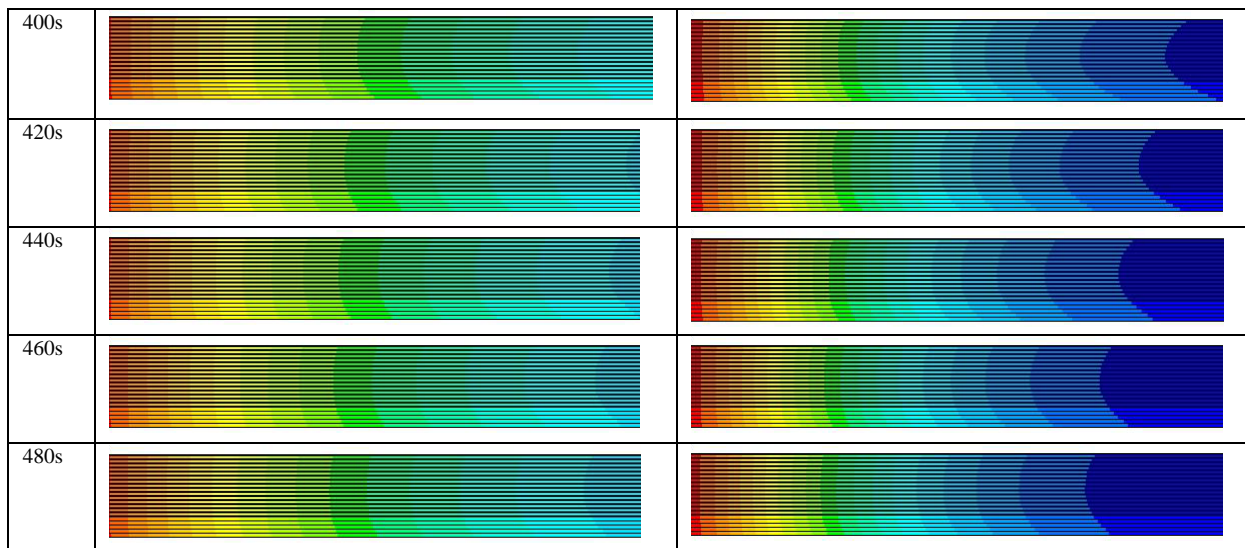


Figure 8. Simulated Contours of CO and NO Mass Fraction inside Catalytic Converter at Time Elapsed After Engine Cold Start

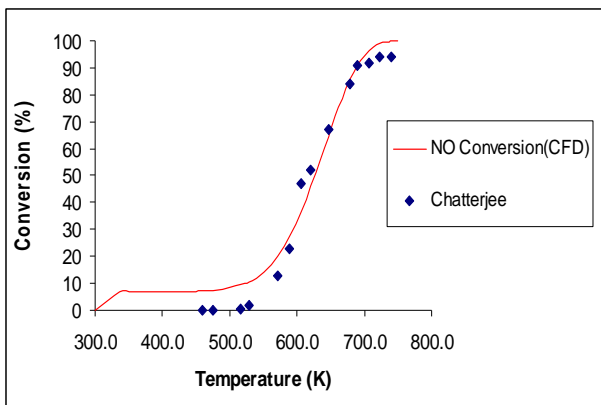


Figure 9. Conversion of NO at Stoichiometric Conditions with Increasing Temperature of TWCC. Experimental data from Chatterjee et al. (2001)

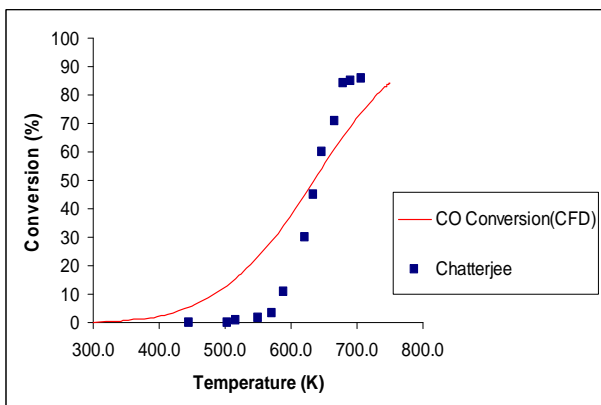


Figure 10. Conversion of CO at Stoichiometric Conditions with Increasing Temperature of TWCC. Experimental data from Chatterjee et al. (2001)

#### 4.1.2 Monolith Optimal Length Design Using Simulation

The design of monolith’s length can be assisted using the CFD simulation. A catalytic converter’s fractional conversion is dependant on the length if other factor is unchanged. The simulation showed that the monolith’s temperature was rising gradually, even after light-off, in

axial direction as shown in Figure 7. The downstream area of the monolith increased further and accelerated the NO and CO conversion in the monolith until the whole monolith achieved light-off temperature. A longer monolith may reduce time to achieve high NO and CO conversion compared to a shorter monolith. However, a longer monolith will be more expensive since material and catalyst quantities are more.

#### 4.1.3 Determination of Length of Monolith

For NO, when the rear of monolith achieved NO light-off temperature at about 310°C at t = 380 s as shown in Figure 7, mass fraction of NO at the rear monolith was below 10ppm which was correspond to conversion efficiency of 97%. The high conversion value was confirmed by the NO contour profile in Figure 8. At steady state, the NO mass fraction inside the monolith became minimal at length 0.13 m along the X axis of monolith as shown in Figure 11.

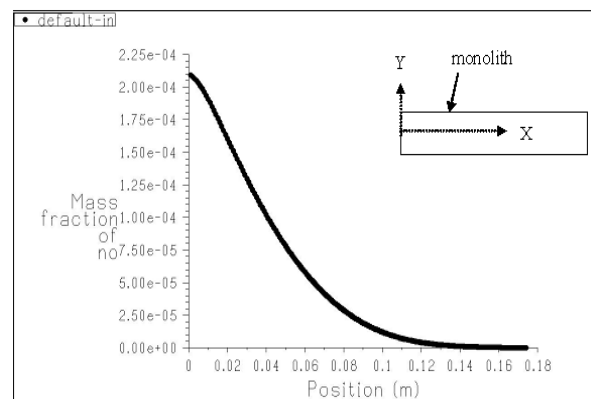


Figure 11. NO mass fraction profile along X axis of monolith at steady state

For CO conversion, mass fraction of CO at the rear monolith became consistent at t = 420 s as shown by the CO contour profile in Figure 7. At steady state, the CO mass fraction inside the monolith gradually lowered to minimal at end of the monolith as shown in Figure 12.

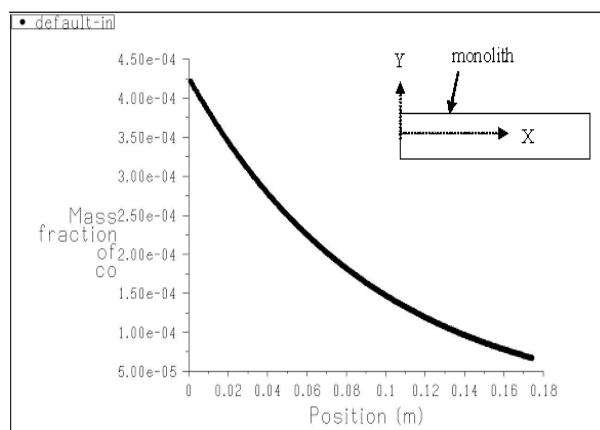


Figure 12. CO mass fraction profile along X axis of monolith at steady state

#### 4.1.4 Sectional Discussion

As shown in Figures 7 and 11, this monolith with length of 17.5 cm can abate NO to conversion of 0.97 after  $t = 380$  s after cold start. However, at steady state, the same monolith needs only 13 cm to abate NO efficiently. Based on the result, a longer monolith may reduce time to achieve high NO conversion but would not further increase the NO abatement in steady state condition after cold-start.

In considering CO abatement, based on simulated result in Figures 7 and 12, further increase in monolith length may increase the CO conversion at steady state. This can be explained by extra catalysts surface available in the added length which increases the CO adsorption and disassociation.

Designer can use the CFD simulation to predict the suitable monolith length taking into factor of NO and CO conversion efficiency against cost factor. The same CFD simulation also can be used to predict NO and CO conversion with different frontal area of monolith.

## 5. Conclusion

The simulation in CFD Fluent 6.0 to predict NO and CO emissions of a cold start CNGV with catalytic converter were done without coupling with extra CFD modules. The transient thermal distribution of the catalytic converter in cold start operation was simulated satisfactorily in CFD. The simulation program also predicted the light-off temperature of NO conversion at 583K and CO conversion at 523K in cold start operation within the ranges of measured value presented in the literature.

The transient conversion rate of NO in cold start is successfully simulated and predicted by the model in CFD program and agreed well measured value in the literature. The modeling program predicted NO conversion of 99% after light-off at steady state condition. However, the CO transient conversion rate by the model is not well predicted. Nevertheless, the modelling program predicted steady state final CO conversion of 84% which is similar

to measured value in literature. This might be caused by omission of HC conversion reactions in this model which eventually failed to show the effect of NO and HC competing with CO for  $O_2$  in their reactions.

## Nomenclature

$A_r$	Pre-exponential factor
$C_{j,r}$	Molar concentration of each reactant and product species $j$ in reaction $r$ ( $\text{kgmol}/\text{cm}^3$ )
$D_{i,m}$	Diffusion coefficient for species $i$ in the mixture
$E_r$	Activation energy for the reaction ( $\text{J}/\text{kgmol}$ )
$h_i^0$	Standard-state enthalpy
$K_r$	Equilibrium constant for the $r^{\text{th}}$ reaction
$k_{f,r}$	Forward rate constant for reaction $r$
$k_{b,r}$	Backward rate constant for reaction $r$
$J_i$	Diffusion flux of species $i$
$M_i$	Denotes symbol denoting species $i$
$N$	Number of chemical species in the system.
$n'_{j,r}$	Forward rate exponent for each reactant and product species $j$ in reaction $r$
$n''_{j,r}$	Backward rate exponent for each reactant and product species $j$ in reaction $r$
$R$	Universal gas constant ( $\text{J}/\text{kgmol}\cdot\text{K}$ ).
$R_i$	The net rate of production by chemical reaction
$\hat{R}_{i,r}$	Arrhenius molar rate of creation or destruction of species $i$ in reaction $r$ .
$S_i$	The rate of creation by addition from the dispersed phase
$S_i^0$	Standard-state entropy
$P_{\text{atm}}$	Atmospheric pressure (101325 Pa).
$Y_i$	Local mass fraction of each species
$\rho$	Gas density, $\text{g}/\text{cm}^3$
$\gamma_{j,r}$	Third-body efficiency of the $j^{\text{th}}$ species in the $r^{\text{th}}$ reaction.
$\bar{\nu}_r$	Temperature exponent (dimensionless),
$\bar{v}$	Velocity, $\text{cm}/\text{s}$
$\nu'_{i,r}$	Stoichiometric coefficient for reactant $i$ in reaction $r$
$\nu''_{i,r}$	Stoichiometric coefficient for product $i$ in reaction $r$
$\Gamma$	Represents the net effect of third bodies on the reaction rate.

## References

- [1] Kuo, J.C.W, Morgan, C.R. and Lassen, H.G. Mathematical modelling of CO and HC catalytic converter systems. (*SAE Trans.* (1971). Vol. 80, Paper 710289.
- [2] Heck, R.H., Wei, J. and Katzer, R.J. Mathematical modelling of monolithic catalysts. *A.I.Ch.E. J.* (1976) 477-484.
- [3] Young, L.C. and Finlayson, B.A. Mathematical models of the monolithic catalytic converter. Part 2. Application to automobile exhaust. *A.I.Ch.E. J.* (1976b) 343-353.
- [4] Oh, S.H. and Cavendish, J.C. Transients of monolithic catalytic converters: response to step changes in feedstream temperature as related

- to controlling automobile emissions. *Ind. Engng Chem. Prod. Res. (1982) Dev.* 21, 29-37.
- [5] Chen, D.K.S., Oh, S.H., Bissett, E.J. and van Ostrom, D.L. A three dimensional model for the analysis of transient thermal and conversion characteristics of monolithic catalytic converters. *SAE (1988)Paper* 880282.
- [6] Zygourakis, K., Transient operation of monolith catalytic converters: a two-dimensional reactor model and the effects of radially nonuniform flow distributions. *Chem. Engng Sci.* 44,(1989) 2075-2086.
- [7] Hayes, R.E., Kolaczowski, S.T. and Thomas, W.J. Finite element model for a catalytic monolith reactor. *Comput. Chem. Engng* 16, (1992) 645-657
- [8] FLUENT Inc. *FLUENT 6.0 User's Guide*, FLUENT Documentation (2001).
- [9] Siemund, S., Leclerc, J.P., Schweich, D., Prigent, M. and Castagna, F. Three-way monolith converter: simulations versus experiments. *Chem. Engng. Sci.* Vol. 51, No. 15, (1996) 3709-3720.
- [10] Taylor, W. III. CFD prediction and experimental validation of high temperature thermal behaviour in catalytic converters. *SAE Special Publication*, SP-1455, (1999) 29-42.
- [11] Koltsakis, G.C. and Stamatelos, A.M. Modeling dynamic phenomena in 3-way catalytic converters. *Chem. Engng. Sci.* 54, (1999) 4567-4578
- [12] Jirat, J., Kubicek, M. and Marek, M.. Adsorber-reactor systems for emission treatment from mobile sources. *Chem. Engng. Sci.*, Vol. 56, Issue 4, (2001) 1597-1604
- [13] Koci, P., Marek, M., Kubicek, M., Maunula, T. and Harkonen, M. Modelling of catalytic monolith converters with low- and high-temperature NOx storage compounds and differentiated washcoat. *Chem Engng. Journal*, 97. (2003) 131-139
- [14] Tsinoglou, D.N., Koltsakis, G.C. Missirlis, D.K. and Yakinthos, K.J. Transient modelling of flow distribution in automotive catalytic converters. *Applied Mathematical Modelling*, Vol. 28, Issue 9. (2003) 775-794.
- [15] Hoebink, J.H.B.J., van Gemert, R.A., van den Tillaart, J.A.A. and Marin, G.B. Competing reactions in three-way catalytic converters: modelling of the NOx conversion maximum in the light-off curves under net oxidising conditions. *Chem. Engng. Sci.* 55, (1999) 1573-1581.
- [16] Harmsen, J.M.A., Hoebink, J.H.B.J. and Schouten, J.C. Transient kinetics of ethylene and carbon monoxide oxidation for automotive exhaust gas catalysis: experiments and modeling. *Reaction Kinetics and The Development of Catalytic Processes.* (1999) 101-108.
- [17] Harmsen, J.M.A., Hoebink, J.H.B.J. and Schouten, J.C. Kinetics of the steady-state acetylene oxidation by oxygen over a Pt/Rh/CeO<sub>2</sub>/ - Al<sub>2</sub>O<sub>3</sub> three-way catalyst. *Topics in Catalysis*, Vol. 16/17, (2001) 1-4.
- [18] Jeong, S.J. and Kim, W.S. Simulation of thermal and flow characteristics for optimum design of an automotive catalytic converter. *Chem. Engng. Comm.*, 189: (2002) 1314-1339
- [19] Chakravarty, V.K., Conklin, J.C., Daw, C.S. and D'Azevedo, E.F. Multi-dimensional simulations of cold-start transients in a catalytic converter under steady inflow conditions. *Applied Catalysis A: General.* Vol. 241, Issue 1-2: (2003) 289-306.
- [20] Shuai, S.J. and Wang, J.X. Unsteady temperature fields of monoliths in catalytic converters. *Chem. Engng. Journal*, 100. (2004) 95-107.
- [21] Ramanathan, K., Balakotaiah, V. and West, D.H. Optimal design of catalytic converters for minimizing cold-start emissions. *Catalysis Today*, Vol. 98, Issue 3: (2004) 357-373
- [22] Chatterjee, D., Deutschmann, O. and Warnatz, J. Detail surface reaction mechanism in a three-way catalyst. *The Royal Society of Chemistry. Faraday Discuss.*, 119,(2001) 371-384.
- [23] Heck, R.M., Farrauto, R.J. and Gulati, S.T. *Catalytic Air Pollution Control*, 2<sup>nd</sup> Edition, John Wiley & Sons. Inc., New York, USA. 2002
- [24] Ristovski, Z.D., Morawska, L., Hitchins, J., Thomas, S., Greenaway, C. and Gilbert, D. Particle emissions of compressed natural gas engines. *J Aerosol Sci.* 31, (2000) 403-413.
- [25] Chan, S.H. and Hoang, D.L. Heat transfer and chemical reactions in exhaust system of a cold start engine. *Int. Journal of Heat Transfer* 42, (1999) 4165-4183
- [26] Burch, S.D., Porter, T.F., Keyser, M.A., Brady, M.J. and Micheals, K.F. Reducing cold start emissions by catalytic converter thermal management. *SAE Paper* (1995) 950409.